Brittle plus plastic deformation of gypsum aggregates experimentally deformed in torsion to high strains: quantitative microstructural and texture analysis from optical and diffraction data

M. Zucali, V. Barberini, D. Chateigner, B. Ouladdiaf and L. Lutterotti

Geological Society, London, Special Publications 2010; v. 332; p. 79-98
doi:10.1144/SP332.6

Brittle *plus* plastic deformation of gypsum aggregates experimentally deformed in torsion to high strains: quantitative microstructural and texture analysis from optical and diffraction data

M. ZUCALI[1]*, V. BARBERINI[2], D. CHATEIGNER[3], B. OULADDIAF[4] & L. LUTTEROTTI[5]

[1]*Dipartimento di Scienze della Terra 'Ardito Desio', Università degli Studi di Milano, Via Mangiagalli 34, 20133 Milano, Italy*

[2]*Dipartimento di Scienze Geologiche e Geotecnologie, Università degli Studi di Milano-Bicocca, Piazza della Scienza 4, 20126 Milano, Italy*

[3]*Laboratoire de Cristallographie et Sciences des Matériaux (CRISMAT), Ecole Nationale Supérieure d'Ingénieurs de Caen (ENSICAEN), Université de Caen Basse-Normandie, 6 Bd M. Juin, 14050 Caen, France*

[4]*Institut Laue-Langevin, BP 156, 6 rue Jules Horowitz, 38042 Grénoble Cedex 9, France*

[5]*Department of Materials Engineering, Engineering Faculty, University of Trento, Via Mesiano, 77, I-38100 Povo-Trento, Italy*

**Corresponding author (e-mail: Michele.Zucali@unimi.it)*

Dedicated to the memory of Luigi Burlini

Abstract: This contribution presents a quantitative microstructural analysis of a polycrystalline aggregate of gypsum, deformed in torsion ($T = 70–90$ °C) at γ (shear strain) ranging from 0 to 4.82. Quantitative microstructural analysis is used to compare the evolution of microstructures observed by optical microscope with those obtained from analysis of X-ray and neutron diffraction data. This analysis shows that during experimental deformation, gypsum accommodated strain by brittle and plastic deformation mechanisms, developing Riedel-like microfaults with plastic foliations and crystallographic preferred orientation (CPO). The relations of microstructures show that with increasing strain, the Riedel systems start from *R* planes with an angle of $\approx 30°$ to the Imposed Shear Plane. This angle decreases ($5°–15°$) when strain increases, and *Y* planes develop. Quantitative texture analysis (QTA) shows that S-foliations start developing at low γ and maintain their orientation up to high γ, and that the most active slip system is the (010) along normal to (100) and the [001]-axis. Shape preferred orientation (SPO) of gypsum does not coincide with the theoretical orientation as it does not decrease with increasing strain. This discrepancy is explained by the role of the brittle shear planes that impose a back rotation to gypsum. No brittle to plastic transition occurs. But both plastic and brittle structures contemporaneously accommodate and localize strain.

Many rocks (metamorphic, igneous and sedimentary) show non-random orientation distributions of their crystallites that results in anisotropies of macroscopic physical properties (Turner & Weiss 1963; Wenk 1985; Randle & Engler 2000; Karato 2008). The crystallographic/lattice or shape preferred orientation (SPO) of crystals with respect to macroscopic fabric axes may be attained in response to deformation processes. The interpretation of textures (i.e. crystallographic preferred orientation) in materials (e.g. rocks or rock analogues) relies on a quantitative description of the orientation features. Together with several other texture analysis methods, quantitative texture analysis (QTA) using neutron and X-ray diffraction has been successfully used in recent years to completely describe the crystallographic preferred orientation (CPO) of naturally deformed rocks (e.g. Kocks *et al.* 1998; Leiss *et al.* 2000; Zucali *et al.* 2002; Zucali & Chateigner 2006; Wenk 2006 and references therein).

In this work we present, together with a detailed and complete microstructural analysis, the results of QTA measurements from neutron and X-ray experiments carried out on samples of natural gypsum that were experimentally deformed in torsion at high shear strains and confining pressure, and at various temperatures and strain rates (Barberini *et al.* 2005). The QTA measurements were performed at the ILL neutron facility (Grénoble,

From: SPALLA, M. I., MAROTTA, A. M. & GOSSO, G. (eds) *Advances in Interpretation of Geological Processes: Refinement of Multi-scale Data and Integration in Numerical Modelling*. Geological Society, London, Special Publications, **332**, 79–98. DOI: 10.1144/SP332.6 0305-8719/10/$15.00

France) and at the Laboratoire de Cristallographie et Sciences des Matériaux (CRISMAT), Ecole Nationale Supérieure d'Ingénieurs de Caen (ENSICAEN, France).

The study of the deformation behaviour of minerals that form evaporitic rocks is of great importance because these rocks can easily localize deformation. Several studies have described the structures and behaviour of gypsum deformed under various conditions (Craker & Schiller 1962; Baumann 1984; Panozzo Heilbronner & Olgaard 1987; Harland *et al.* 1988; Ko *et al.* 1995; Stretton 1996; Barberini *et al.* 2005) and the tectonic implications of gypsum dehydration (Heard & Rubey 1966), but only a few have described the microstructural and textural evolution (Levykin & Parfenov 1983; Kern & Richter 1985; Panozzo Heilbronner & Dell'Angelo 1990; Panozzo Heilbronner 1993). Such studies describe the evolution of a preferred orientation of poles to planes (010), perfect cleavage planes, which is parallel to σ_1 (main axial stress). (010) $<001>$ is considered the most common slip plane but others have also been recognized (Muegge 1898; De Meer 1995). The deformation of gypsum has also been studied under various conditions in order to investigate the behaviour under transient drained conditions (Olgaard *et al.* 1995). Moreover, the instantaneous and long-term behaviour of natural gypsum has been studied to understand the traces of dissolution observed in pillars of underground gypsum quarries (Hoxha *et al.* 2006; Castellanza *et al.* 2008) and to model its long-term behaviour (Hoxha *et al.* 2005). Finally, some authors have studied the creep of wet gypsum aggregates, and the relationships with the mechanics of thrust faults and other large-scale structures, associated with oil and gas accumulations (De Meer & Spiers 1995).

Sample description

The studied gypsum samples are cores about 9 mm thick and 7–15 mm long obtained from natural gypsum (gypsum >99%). The specimens (Table 1 and Fig. 1a) were deformed in torsion experiments (Paterson & Olgaard 2000) up to high shear strain values (up to $\gamma = 5$) at a confining pressure of 300 MPa and at various temperatures (from 70 to 90 °C) and strain rates (between 10^{-3} and 10^{-5} s^{-1}) (Barberini *et al.* 2005). Within cylindrical samples deformed in torsion the deformation varies radially from no deformation at the centre of the core to maximum deformation at the outer surface. Therefore, thin sections for microstructural observations were cut as close as possible to the outer cylinder surface (Fig. 1b).

Table 1. *Experimental details of the studied samples*

Sample	Shear strain (γ)	Shear strain rate (s^{-1})	Temperature (°C)	Drained/undrained	Gypsum/bassanite	Analytical techniques*
VGO	–	–	–	–	G	OM–NT–XT
V4	0.36	5×10^{-5}	127	D	B + G	OM
V7	0.49	5×10^{-5}	70	U	G	OM–NT–XT
V6	1.12	up to 1×10^{-4}	90	U	G + B	OM
V8	1.19	1×10^{-4}	90	U	G + B	OM–NT–XT
V13	1.78	1×10^{-4}	90	D	G + B	OM
V15	1.80	1×10^{-4}	70	D	G	OM
V9	2.49	1×10^{-4}	90	U	G + B	OM
V18	2.59	up to 6×10^{-4}	70	D	G	OM–NT–XT
V14	2.61	2×10^{-4}	90	D	G	OM–NT–XT
V11	2.89	6×10^{-4}	90	D	G	OM
V10	4.07	2×10^{-4}	90	D	G	OM–NT–XT
V16	4.11	1×10^{-4}	70	D	G	OM–XT
V20	4.82	1×10^{-4}	70	D	G	OM–NT

*OM, optical microscopy; NT, neutron texture; XT, X-ray texture.

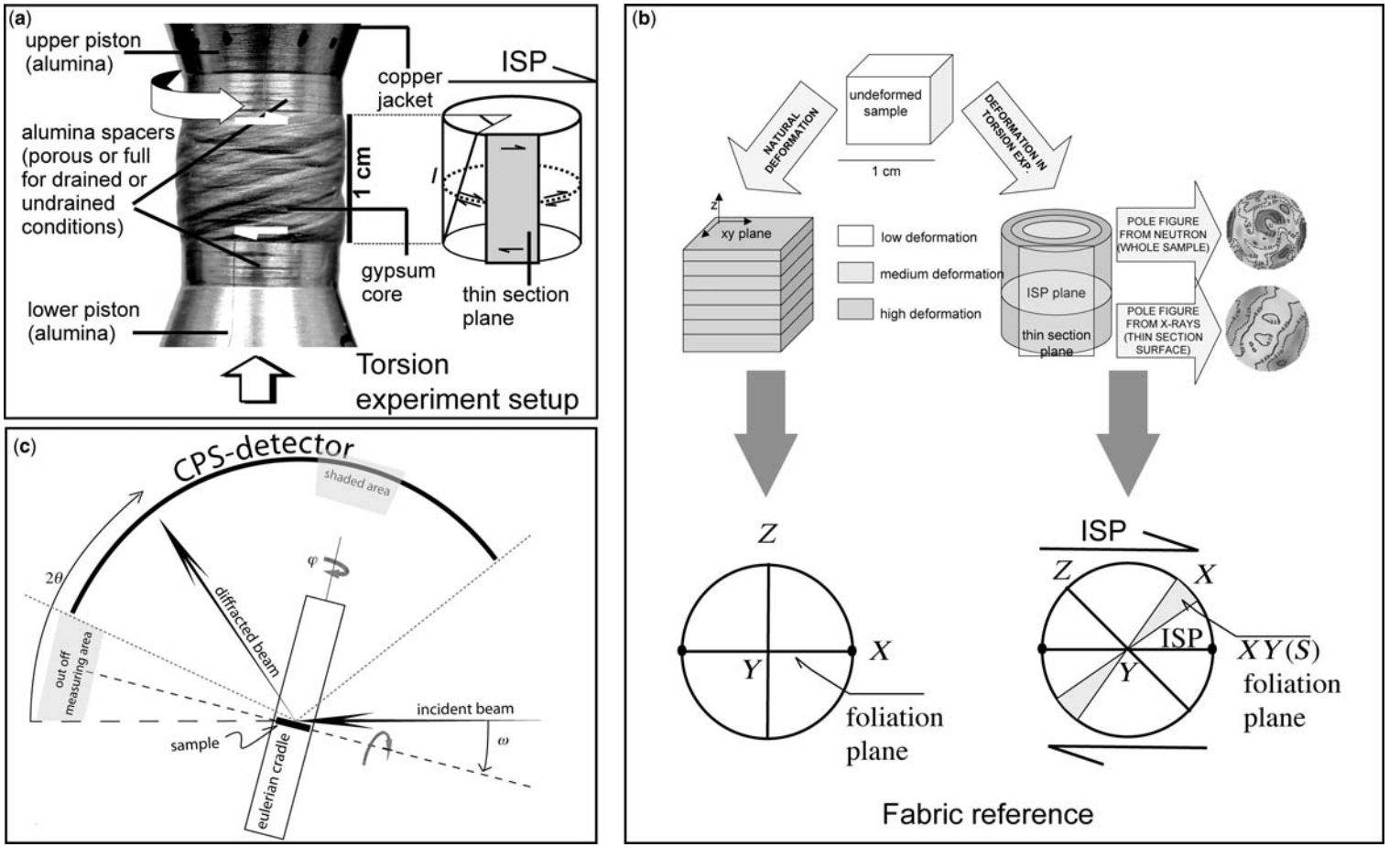

Fig. 1. (**a**) Deformation experiments in Paterson gas-medium HPT apparatus equipped for torsion testing (ETH, Zürich, Switzerland). Details about these experiments are in Barberini *et al.* (2005). (**b**) Top: comparison between deformation geometry in natural samples, and torsion samples and effect of torsion deformation on pole figures (from neutron and X-ray). Bottom: relationships between fabric reference and sample reference within pole figures. (**c**) Geometry of the performed texture measurements (neutron and X-ray) using the Curved Position Sensitive detector (CPS). ISP, Imposed Shear Plane; *X*, *Y*, *Z*, principal fabric axes; *XY* (S) plane, foliation plane.

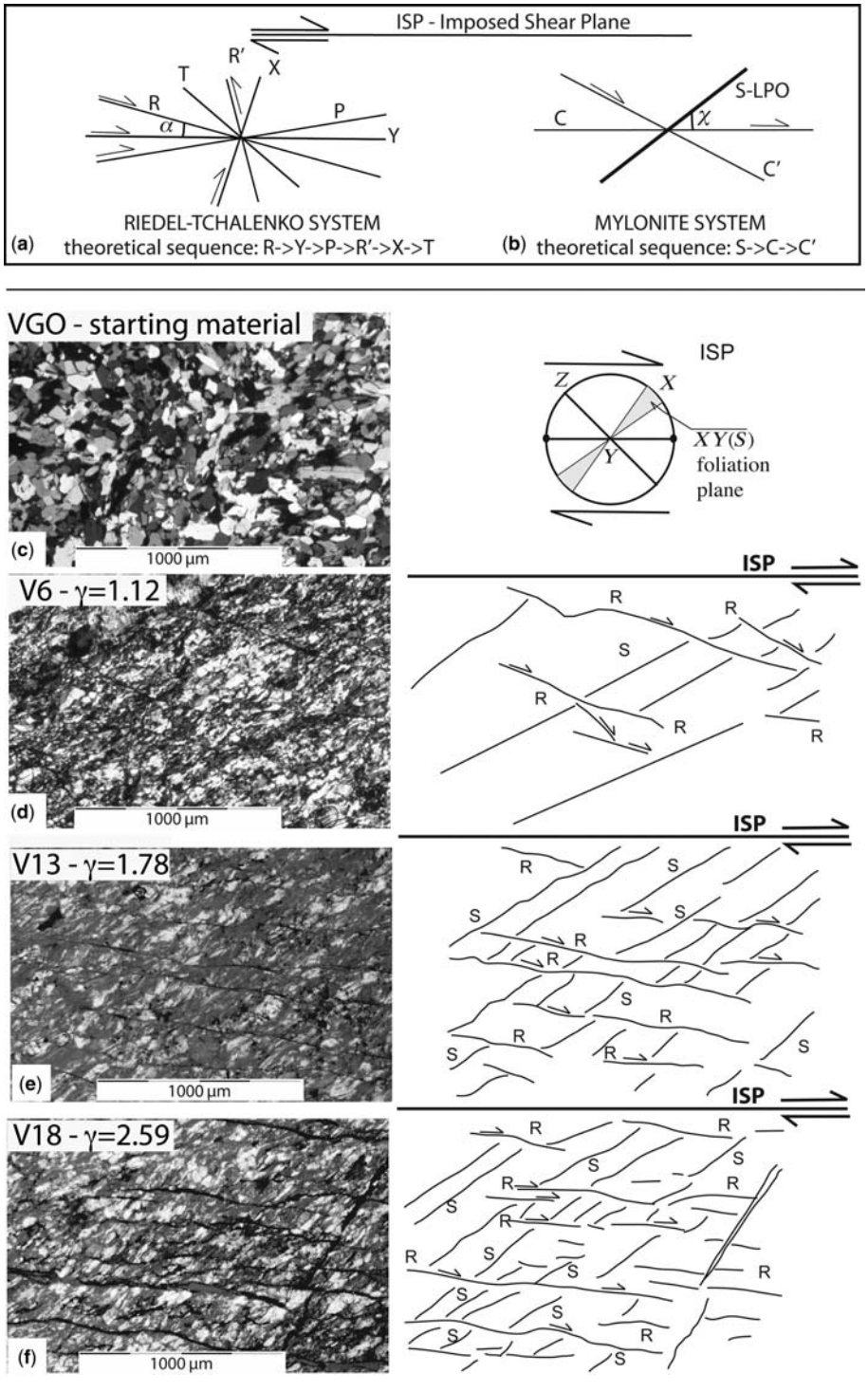

Fig. 2. Description of (**a**) brittle and (**b**) plastic deformational systems affecting the deformed samples. (**c**)–(**f**) Microphotographs (left) and microstructural analysis (right) of gypsum samples deformed in torsion up to $\gamma = 2.59$. The starting material (c) shows an heterogeneous grain size distribution (20–250 μm) and a polygonal fabric with only occasional SPO. At $\gamma = 1$–2, (d) and (e), undulose extinction and kink bands affect an increasing number of grains of

Microstructural analysis

The sample reference frame is defined by the Imposed Shear Plane (ISP) (Fig. 1), which is the plane perpendicular to the optical images and parallel to the long edge of the images, with the rotation axis of the torsion experiments being the vertical axis of the images (Figs 2 & 3). The three fabric axes $X-Y-Z$ define the fabric reference frame (Figs 1b & 2c), with the SPO (S foliation) being close to the XY plane (Passchier & Trouw 1996). Grain-size analysis (Fig. 4a) has been performed using digital microphotographs analysed with the software ImageJ (Rasband 1997–2008; Abramoff *et al.* 2004).

The deformed samples show different microstructures related to their different shear strain states. Here the microstructural features of main strain steps are reported (Figs 2 & 3).

- The starting material (sample VGO, Fig. 2c) is characterized by a heterogeneous grain-size distribution from 20 to 250 μm, with mean values at about 80 μm (Fig. 4a). It generally shows a polygonal fabric with few exceptions. Undulose extinction occurs within a few small grains, while larger grains display homogeneous extinction or subgrains with straight boundaries. Large grains are also characterized by twins, and a slight SPO sometimes occurs within small volumes.
- At low levels of shear strain ($\gamma < 1.00$), undulose extinction is visible within the largest grains where kink bands also formed; within small grains, undulose extinction starts and several grain boundaries show lobate shapes. Grains size does not change, ranging from 20 to 250 μm, with mean values at about 70–80 μm (Fig. 4a).
- At $\gamma = 1.00–2.00$ (Fig. 2d, e), the development of undulose extinction and kink bands affects an increasing number of grains of different sizes. The grain size still ranges between 20 and 200 μm, but mean values decrease at 60 μm (Fig. 4a). Kink bands are mainly developed within larger grains, associated with the SPO, mechanical twinning and undulose extinction. The SPO of flattened grains starts to develop at an angle of about 30°–45° (bottom left – top right) with respect to the ISP; it becomes stronger with increasing strain and is also associated with the lattice preferred orientation (LPO). Small grains are characterized by undulose extinction and subgrains' preferred orientation. Narrow disjunctive dark planes occur at a small (<10°) angle to the ISP; these planes are generally discontinuous and enclose single grains or aggregates of grains that show undulose extinction and subgrains, and may show an SPO marked by elongated gypsum grains (bottom left–top right).
- At $\gamma = 2.00–3.00$ (Figs 2f & 3a, b) shear bands become more penetrative and continuous, forming two distinct systems of brittle shear planes at angles of about 10°–20° to the ISP. Gypsum aggregates display a strong SPO (S foliation) at a high angle (>45°) to the shear bands parallel to the ISP (i.e. bottom left–top right) and the grain-size ranges decrease, ranging from 10 to 150 μm with mean values of less than 50 μm (Fig. 4a). Gypsum aggregates are characterized by strong undulose extinction, subgrain development, and a LPO of old elongated grains and newly formed crystals. Kink bands and mechanical twinning occur within large grains (>100 μm). Grain-size reduction processes are active as the grain size ranges from 10 to 50 μm.
- At $\gamma > 4.00$ (Fig. 3c–e) the grain-size reduction increases and the mean grain size is generally <50 μm (Fig. 4a). The LPO and SPO of the grain aggregates become more defined and marks a well-defined S foliation, which has an angle of about 45° with respect to the ISP. The shear planes define two sets of planes mostly parallel to the ISP that produce shear lenses; the S foliation, marked by the SPO and LPO of gypsum, is cut by these shear planes. Single gypsum crystals occur as elongated strips parallel to the S foliation and appear slightly curved, showing 'S'-type symmetry and giving rise to two main SPO orientations: one at a low angle with the ISP, occurring near the shear planes; and the second at a higher angle, far from the shear planes. Very few large grains (30–120 μm) may preserve kink bands and twinning.

Deformational systems

All samples show two sets of microstructures that correspond to two different deformational regimes: (I) brittle (Fig. 2a) and (II) plastic (Fig. 2b) regimes (Passchier & Trouw 1996).

Fig. 2. (*Continued*) different size. Grain size ranges between 20 and 100 μm. SPO (with associated LPO) of flattened grains develops at an angle of about 30°–45° (bottom left–top right) with respect to the ISP. At $\gamma = 2–3$ (f) gypsum aggregates, characterized by strong undulose extinction and subgrains development, show strong SPO at high angles (>45°) with respect to ISP. Old elongated grains and newly formed crystals both show LPO. Grain size is now reduced to 10–50 μm. Shear bands become more penetrative and form two systems of brittle shear planes at an angle of 10°–20° with respect to ISP.

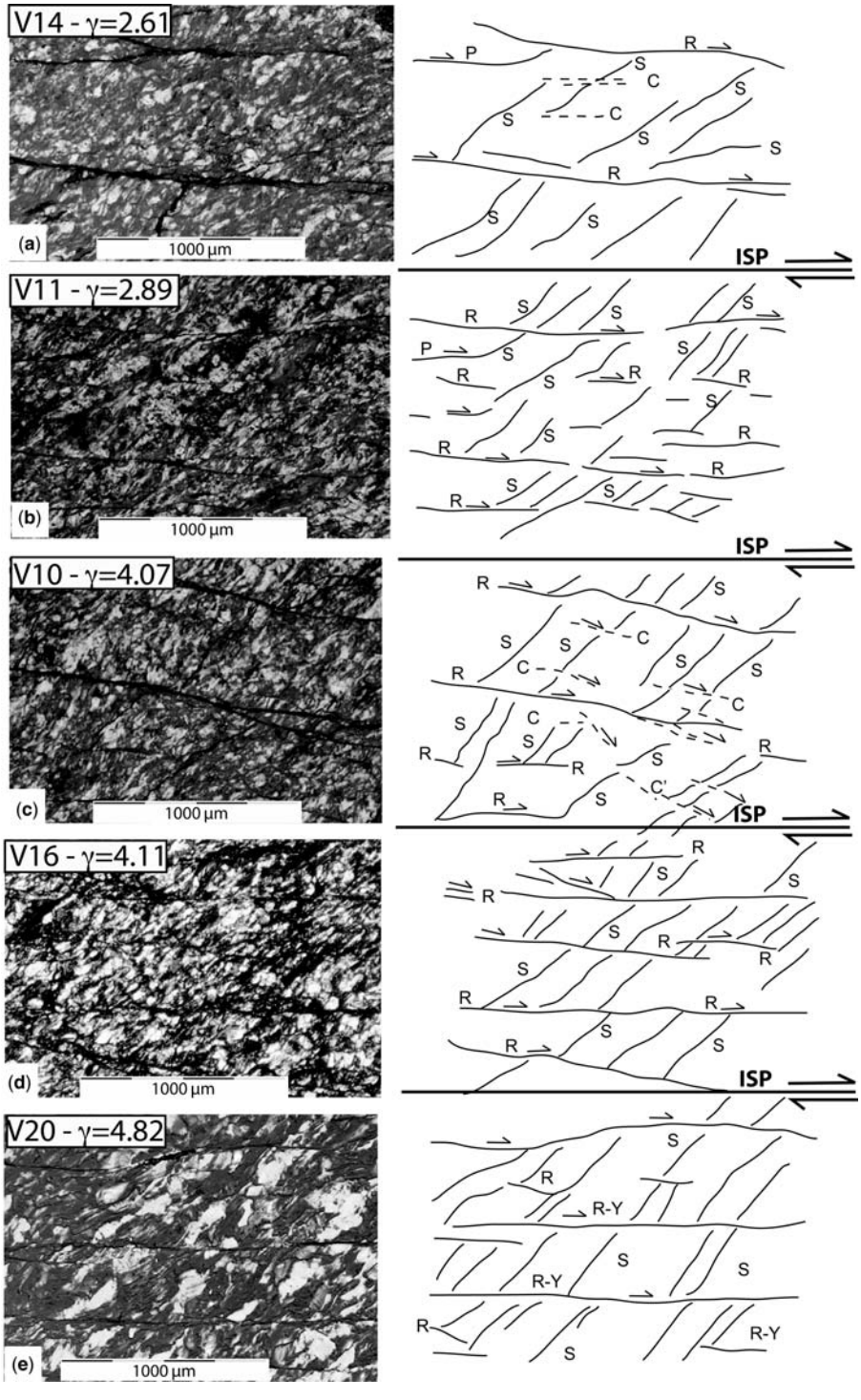

Fig. 3. Microphotographs (left) and microstructural analysis (right) of gypsum samples deformed in torsion up to $\gamma = 4.82$. At $\gamma = 2–3$ (**a**) and (**b**) gypsum aggregates, characterized by strong undulose extinction and subgrains development, show strong SPO at high angles ($>45^{\circ}$)with respect to ISP. Old elongated grains and newly formed

The first system of microstructures is defined by narrow and localized shear planes marked by disjunctive planes (dark planes in Figs 2 & 3). These shear planes evolve from low to high shear strain values constituting an evolving Riedel-like shear system (Fig. 2a) similar to those described by Tchalenko (1970) at various scales.

The second system is defined by a set of two foliations marked by an SPO and LPO of gypsum grains that follow the scheme of development within mylonitic shear zones (Fig. 2b). The schematic drawings combined with microphotographs in Figures 2 and 3 summarize the evolution of both the brittle (Fig. 2a) and the plastic (Fig. 2b) shear systems with increasing shear strain.

Brittle (Riedel-like) and plastic (mylonitic-like) structures

In this section we will compare the classical models of structure development within localized shear zones (Snoke *et al.* 1998), either brittle (Riedel–Tchalenko-like, Fig. 2a) or plastic (Fig. 2b) systems, with the observed microstructures corresponding to increasing shear strain (γ). The shear strain is measured, for an isotropic homogeneous cylindrical specimen of diameter, d, length, l, and angular displacement (θ) (Fig. 1a), as $\gamma = d\theta/2l$, (Paterson & Olgaard 2000). The angular relationship between planar structures and the ISP are shown [α (angle between ISP and R plane) and χ (angle between ISP and S foliation) angles] in Figure 2a, b. In the Riedel scheme (Fig. 2a) the different planes form different angles with the ISP and are also characterized by a specific shear sense (kinematic). In Figure 2b, the angular relations between the foliations and the ISP are shown. Figure 4 shows the evolution of α and χ with respect to shear strain.

- At $\gamma = 0$–1.00 (Fig. 2c) no distinctive structure develops.
- At $\gamma = 1.00$–1.50 (Fig. 2d) both R and S planes (Fig. 2a, b) develop. S planes are characterized by an SPO and LPO, and occur at a χ angle of about 45° (Fig. 4a). The R planes cut the S planes with a dextral shear sense as shown by small displacements along the R planes and α occurring at high values with the ISP.
- At $\gamma = 1.50$–2.00 (Fig. 2e) S planes develop at χ angles of less than 45° (Figs 2e & 4a), and are marked by an SPO and LPO of strained gypsum grains. The R planes show dextral shear sense outlined by the displacement of gypsum grains marking the S planes, and dissolution occur along the R planes, as shown by sharp truncations of such gypsum grains. A few R splays also occur, and the α angles are generally lower than at lower γ values (Fig. 4a).
- At $\gamma = 2.00$–2.50 (Fig. 2f) the S planes are marked by well-developed SPO and LPO of gypsum grains, and χ angles ranging from 20° to 40°. The R planes are more penetrative and occur at smaller α angles. Towards the R planes, the S planes are gently deflected, showing a more plastic behaviour and allowing the interpretation of a dextral shear sense. Several smaller R planes occur, organized in an en-echelon-type geometry. α angles become smaller and few fractures occur parallel to both the R and S planes.
- At $\gamma = 2.50$–3.00 (Fig. 3a, b) the S planes are still well developed and are at high angles ($\approx$45°) to the ISP, but they are also highly deflected by small C-type (Fig. 2b) shear planes that occur at very low angles with the ISP (Fig. 3a, b). These features correspond to the S–C geometry of mylonitic shear zones. Along the C planes small undeformed (no undulose extinction) and equigranular gypsum grains occur. R planes develop at very low angles with the ISP as the α angles approach 0 (Fig. 4b), becoming Y-type planes of the Riedel scheme (Fig. 2b). Along these sets of R–Y planes, diffuse dissolution occurs. A few R–Y splays and P planes also occur.
- At $\gamma > 4.00$ (Fig. 3c–e) S planes marked by the SPO and LPO of gypsum are penetrative, and describe an angular relation with the ISP of about 30°–45° (Figs 3c–e & 4). C planes also develop with a dextral shear sense, and seem to be associated with the development of layers of small strain-free grains of gypsum probably due to dynamic recrystallization. The R–Y planes are characterized by very low α values and the development of shear lenses. Along a few small planes oriented within a C'-type geometry, a strong LPO of gypsum occurs; several R planes also occur with the same orientation, suggesting a plastic precursor to this second generation of R planes.

Figure 4b shows the evolution of α (left) and χ (right) with increasing γ with respect to the ISP. The theoretical evolution of the R planes with respect to ISP should correspond to a decreasing of α as γ

Fig. 3. (*Continued*) crystals both show LPO. Grain size is now reduced to 10–50 μm. Shear bands become more penetrative and form two systems of brittle shear planes at an angle of 10°–20° with respect to ISP. At $\gamma > 4$, (**c**)–(**e**), the LPO and SPO of the grain aggregates is more defined and marks a well-defined S foliation, forming an angle of about 45° to the ISP. Shear planes define two sets of planes mostly parallel to the ISP.

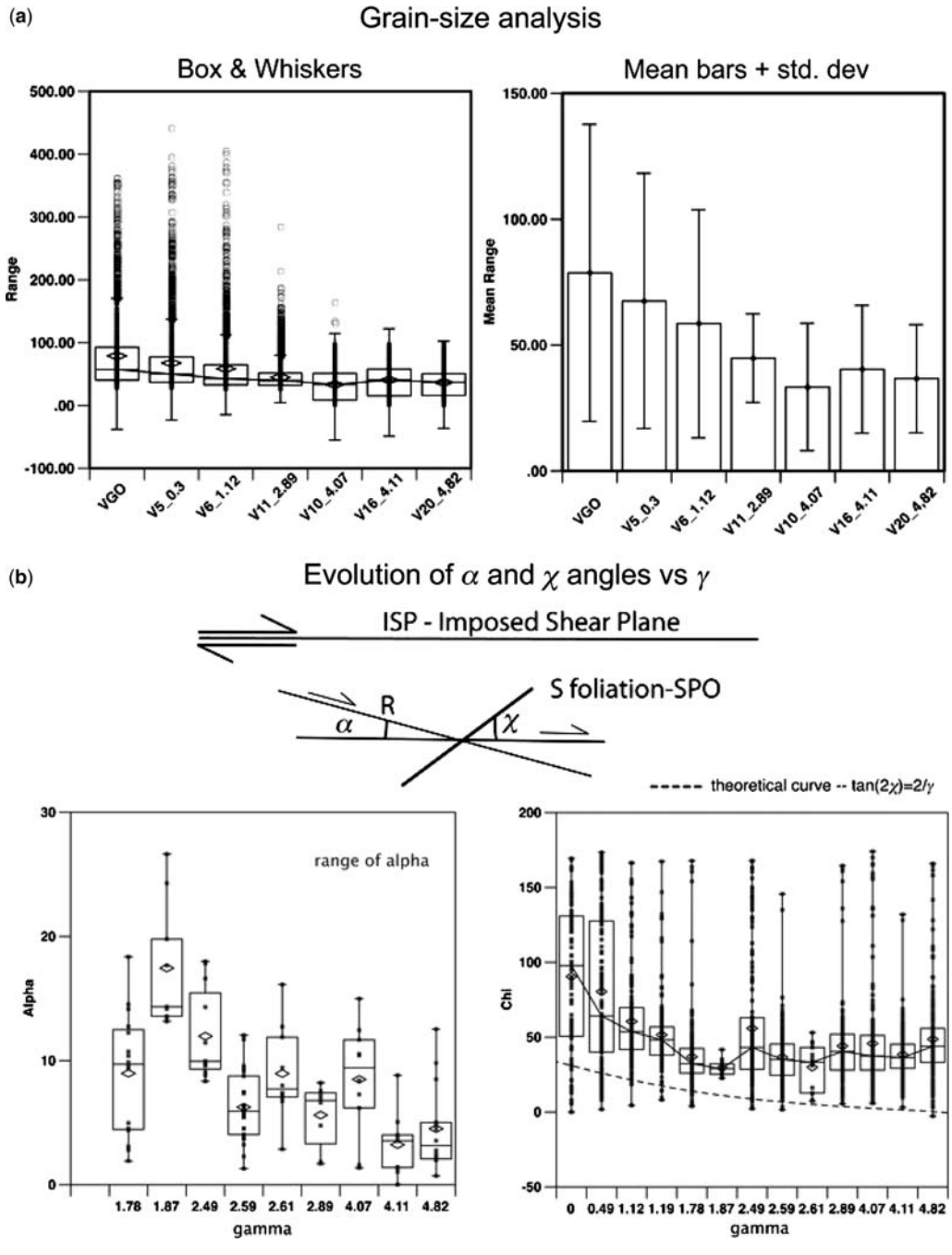

Fig. 4. (**a**) Box and whiskers representations (left) of the grain-size distribution with respect to γ values; mean bars and corresponding standard deviations of the grain-size distribution; both diagrams clearly show the decrease in grain size with the increase in γ values. (**b**) Diagrams show the evolution of α (left) and χ (right) angles v. γ intervals. α values increase at first (up to γ around 2) and then show a decreasing trend. χ values slightly decrease at first for increasing γ values, then, due to the counterclockwise rotation along $Y-R$ shear bands they oscillate at around $40-45^{\circ}$ values, never reaching the theoretical curve of the finite strain long axis (dashed line).

increases, as supported by analogue modelling and field observations (Snoke *et al.* 1998). Such a decrease in α corresponds to the transition from *R* to *Y* planes that lie parallel to the ISP. This theoretical evolution is in agreement with the development and evolution of *R* planes within gypsum aggregates deformed in torsion from low to high γ (Fig. 4b, left). The evolution of the χ angles, which correspond to the angle between the *S* foliation or SPO of grains and the ISP, should follow the theoretical curve of the finite strain long axis as expected for a shear zone (Fig. 4b right). Whereas the theoretical curve shows a continuing decrease of χ with increasing γ, the actual χ values measured for the studied samples from γ values from 0 to 4.82 do not follow this function, and stabilize at values of 40°–45°. Such discrepancies from the theoretical curve may be related to the concurrence of the deformation mechanisms that were accommodating strain. Microstructural analysis showed that the shear bands were active from the beginning of deformation ($\gamma < 0.5$) and controlled the orientation of grains by imposing shear along the bands. In fact, grains close to the shear bands (*R* or *Y*) are deflected towards the shear band line, and the corresponding χ values are generally lower than those measured on grains far from shear bands. The grains that occupy the regions between two shear bands record a back rotation (i.e. counterclockwise) as imposed by sinistral shear, leading to grains characterized by high χ values. Meanwhile, simple shear deformation involves various deformation mechanisms acting during the evolution from low to high γ; kinking, twinning and passive rotation dominate at low strains, while at higher strains dynamic recrystallization and grain-size reduction (Fig. 4a) become more important and overprint pre-existing microstructures (Barberini *et al.* 2005). Such progressive change to plastic flow does not dominate the entire deformed volume, as shown by the discrepancies between the theoretical and practical finite strain curves (Fig. 4b), with frictional flow along shear bands making up the majority of the overall deformation. Kinking occurs in large grains oriented at about 30°–60° to the ISP.

Quantitative neutron and X-ray diffraction texture analyses

In order to use QTA to compare different samples independently of the grain size, phase ratio and porosity, normalization of the pole figures is needed (Bunge & Esling 1982). This normalization can be obtained via the refinement of the orientation distribution function (ODF), which holds information about the texture intensity and all components of the texture. The measurement of a single pole figure allows only a limited quantitative analysis as it only shows the orientation distribution and the intensity of the preferred orientation from the corresponding crystallographic planes. The crystallographic recalculation of several pole figures from different crystallographic planes according to their crystal structure in the ODF allows a complete quantitative texture analysis of the specific mineral phase. Measuring single pole figures does not allow a quantitative texture analysis because a single pole figure can be obtained by many different ODFs, meaning that the interpretation of the texture from a single pole figure is doubtful. In this study we performed QTA using neutron and X-ray diffraction data. Neutron diffraction data and refined texture hold information about the whole sample (i.e. volumes of about 1 cm^3), while X-rays, due to their low penetration capabilities, are suitable to investigate the marginal domains of the samples. QTA was used to reconstruct the LPO of preferred planes of slip within gypsum grains involved in torsion experiments.

Direct numerical integration is not suitable for a reliable ODF determination because the relatively low 2θ resolution gives rise to peak overlaps, which we resolved using a combination of Rietveld and texture analyses. The Rietveld texture analysis (Matthies *et al.* 1997) has the capacity to separate exact and/or strong overlaps. A Rietveld texture analysis (Lutterotti *et al.* 1997) was performed for all patterns using the software package MAUD (Lutterotti *et al.* 1999). MAUD uses a Rietveld core routine to compute spectra and a so-called Le Bail algorithm (Matthies *et al.* 1997) to extract the differences between random and textured intensities for each computed peak. These spectra are the basis of computing the ODF using the eWIMV algorithm (Morales *et al.* 2002; Lutterotti *et al.* 2004). The obtained ODF was then introduced into the cyclic Rietveld refinement. The new refined parameters were used for a new eWIMV cycle to correct the ODF. Several cycles of refinement were performed to converge towards a final characterization of the material. The refinement quality was assessed by comparison of the experimental and recalculated diagrams, and by the reliability factors as exhaustively described by Chateigner (2005): **RP** for the ODF refinement (Lutterotti *et al.* 1997), and **RB** and **Rw** for the Rietveld refinement (Young & Wiles 1982). As a starting model for the gypsum structure, we used the $A2/a$ space group and cell parameters $a = 6.28$, $b = 15.20$, $c = 6.52$ and $\beta = 127.414$ (Pedersen & Semmingsen 1982; Schofield & Knight 1996; Boeyens & Ichharam 2002; Gražulis *et al.* 2009). This model allowed complete indexing of the diffracted lines, implying that no extra phase was present in the specimens.

Table 2. *Samples and corresponding γ values with reference to reliability factors, goodness of fit, χ^2, texture strength (F^2 in mrd^2) and texture calculation type*

Sample	γ	RW (%)	RB (%)	Rwpb (%)	Rpb (%)	Rexp	χ^2	F^2 (mrd^2)	ewimv
X-ray									
VGO	0	46.88	36.61	76	49.6	21.78	4.62	1.45	y
V7	0.49								
V8	1.19	20.55	16.16	23.77	18.55	10.64	3.72	1.42	y
V18	2.59	21.13	16.55	21.94	17.24	15.6	?	1.4	y
V14	2.61								
V10	4.07	20.36	15.96	21.61	17.03	15.55		1.482	y
V16	4.11	20.53	15.87	22.41	16.51	14.82	1.9	1.63	y
V20	4.82								
Neutron									
VGO	0	11.78	8.95	27.49	15.05	6.41	3.09	0.54	y
V7	0.49	13.23	10.37	26.11	15.8	9.36	1.96	1.37	y
V8	1.19	9.36	7.39	15.39	10.16	6.09	3.38	1.29	y
V18	2.59	14.83	11.68	29.35	18.12	9.51	2.25	1.83	y
V14	2.61	13.04	10.21	26.41	15.93	8.86	2.16	1.39	y
V10	4.07	10.11	8.08	15.09	11.15	5.39	3.49	1.62	y
V16	4.11								
V20	4.82	7.98	6.37	13.3	9.5	3.04	6.86	1.46	y

ODF refinement estimators: RW, Intensity weighted factor; RB, R-Bragg factor. Profile refinement estimators: Rwpb, R-weighted pattern factor; Rpb, R-pattern factor; Rexp, R expected (=1 optimal). ewimv, entropy-WIMV texture model.

The cell parameters were refined during combined analysis (Table 2), but the atomic positions were not, and the crystallite sizes were kept fixed at 1000 Å. No peak shifts were observed during χ rotation of the samples, indicating that only very low levels of residual stresses, if any, were incorporated in the material.

Neutron diffraction

Neutron diffraction experiments were carried out at the Institut Laue Langevin (ILL, Grénoble, France) high flux reactor using the Position Sensitive Detector of the D20 beamline. The detector spans a 2θ range of 153.6° with a resolution of 0.1°, and the neutron wavelength is monochromatized to $\lambda = 2.41$ Å. An Eulerian cradle allows the χ and ϕ angles' rotations (Fig. 1c). Scans were operated from $\chi = 0°$ to 90° at steps of 5° using a fixed incidence angle, ω, of 10° [corresponding to the (020) Bragg position] and from $\phi = 0°$ to 355° (steps of 5°) (Fig. 5). Diffraction data were collected for 4 s. The samples used were the cylindrical specimens deformed in torsion.

X-ray diffraction

X-ray diffraction texture measurements were carried out at the Laboratoire de Cristallographie et Sciences des Matériaux (CRISMAT), Ecole Nationale Supérieure d'Ingénieurs de Caen (ENSICAEN, France), using a Huber four-circle goniometer (closed eulerian cradle $+\theta{-}2\theta$ movements) mounted on an INEL X-ray generator, and Cu Kα wavelength monochromatized by an incident flat graphite monochromator. A curved position sensitive detector with a 2θ resolution of 0.03° (INEL CPS-120) was used to acquire complete diffraction patterns at different sample orientations in the 2θ range of 0°–120° (Fig. 5). The flat samples were measured in reflection geometry. The incident angle on the sample, ω, and the CPS position were chosen in order to get the maximum coverage of the orientation space. The spectra were measured using φ values from 0° to 355°, and χ values from 0° to 60°, at incremental steps of 5° for both angles. Each pattern was acquired for 120 s. The irradiated surface, which was the surface of the cylindrical specimens deformed in torsion from where the thin section was cut (Fig. 1a), was increased by oscillations of the sample perpendicular to the lineation direction (± 3 mm of amplitude).

Assessment of refinement reliability. Table 2 shows the reliability factors for the refinement of the studied samples. Using X-ray diffraction data, all R-factors (reliability factors) of Rietveld and ODF refinement show tendencies toward lower values for γ values above 1.00, while neutron analyses do not show this evolution. This can be attributed to the largest grain sizes for lower γ values, which give rise to grain statistic effects when using

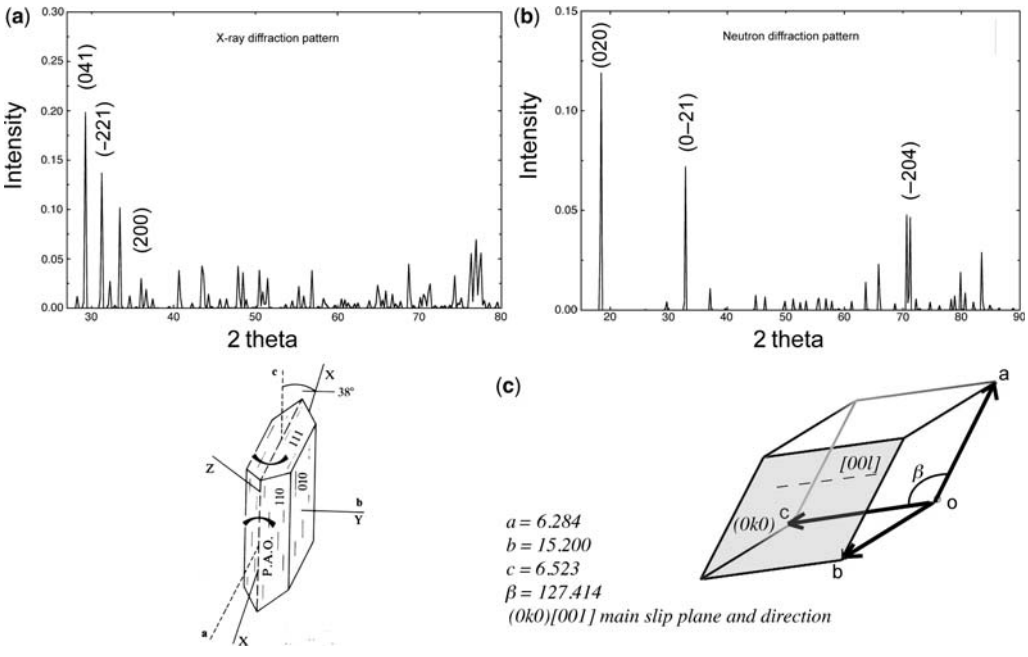

Fig. 5. Theoretical diffraction pattern for gypsum structure (Boeyens & Ichharam 2002) for (**a**) X-ray and (**b**) neutron. In (**c**) the structure of gypsum is represented also showing the main slip plane and direction (Muegge 1898).

X-rays, while neutron measurements still probe enough grains (Zucali *et al.* 2001). Overall, the reliability factors indicate a reasonably good refinement both of diagrams and ODFs for comparable texture strength levels (Chateigner 2005) ranging up to $F^2 = 1.9\ \mathrm{mrd}^2$ (multiple of random distribution), which represent moderate textures. The goodness-of-fit values range from around 1.9 for most of the samples to 4.6 for the worst case, with average values also in favour of neutron analysis. The average values obtained in this work are comparable to values reported in the literature.

Before discussing the QTA data it is important to emphasize that neutron data reflect the LPO of the whole sample, meaning that any PF represents orientations related to the entire sample that corresponds to the complete γ range from the core (minimum) to the edges (maximum). Considering the distribution of shear deformation within a core sample deformed in torsion (Fig. 1b), which is at a maximum at the outer surface and almost zero at the cylinder axis, the obtained textures are the average texture (Fig. 6) and the maximum texture in the external deformed area is probably underestimated. Neither a one-to-one nor a linear relationship between the deformation ratio and the deformed volume fraction from the core to the edge was revealed in the diffracted intensities. Moreover, the surface of the shear zone is not planar, as it would be in a 1 cm edge cube of a naturally deformed rock, but rather corresponds to the cylinder's outer surface. Some of the artefacts (small circles) observed in the pole figures might be due to this rather complex geometry (Fig. 6). Even with such strong limitations the pole figures obtained from neutron data (Fig. 6, left) reproduce well the LPO of gypsum aggregates if compared with pole figures from X-ray data (Fig. 6, right). In addition, at extreme conditions (e.g. very low or zero strain values; high strain values) the pole figures obtained from neutron data due to larger irradiated volumes better characterize the sample textures.

QTA results: X-ray diffraction data

The starting material shows an unexpected LPO with its maximum parallel to the *Y*-axis. At $\gamma < 1.50$, X-ray pole figures show a preferred distribution of the (010) close to the *Z*-axis, and the corresponding (001) and (100) poles roughly aligned along the *XY* plane. At higher γ (>2.5) values, the (010) poles become stronger and are close to the *Z*-axis, with progressive localization of the (100) and (001) poles on a circle perpendicular to (010) (Fig. 7). Starting from these γ values, recalculated pole figures show a stronger (001) pole density maximum with (001) poles aligning at 90° from the *Z* fabric axis and dispersed within about 30°

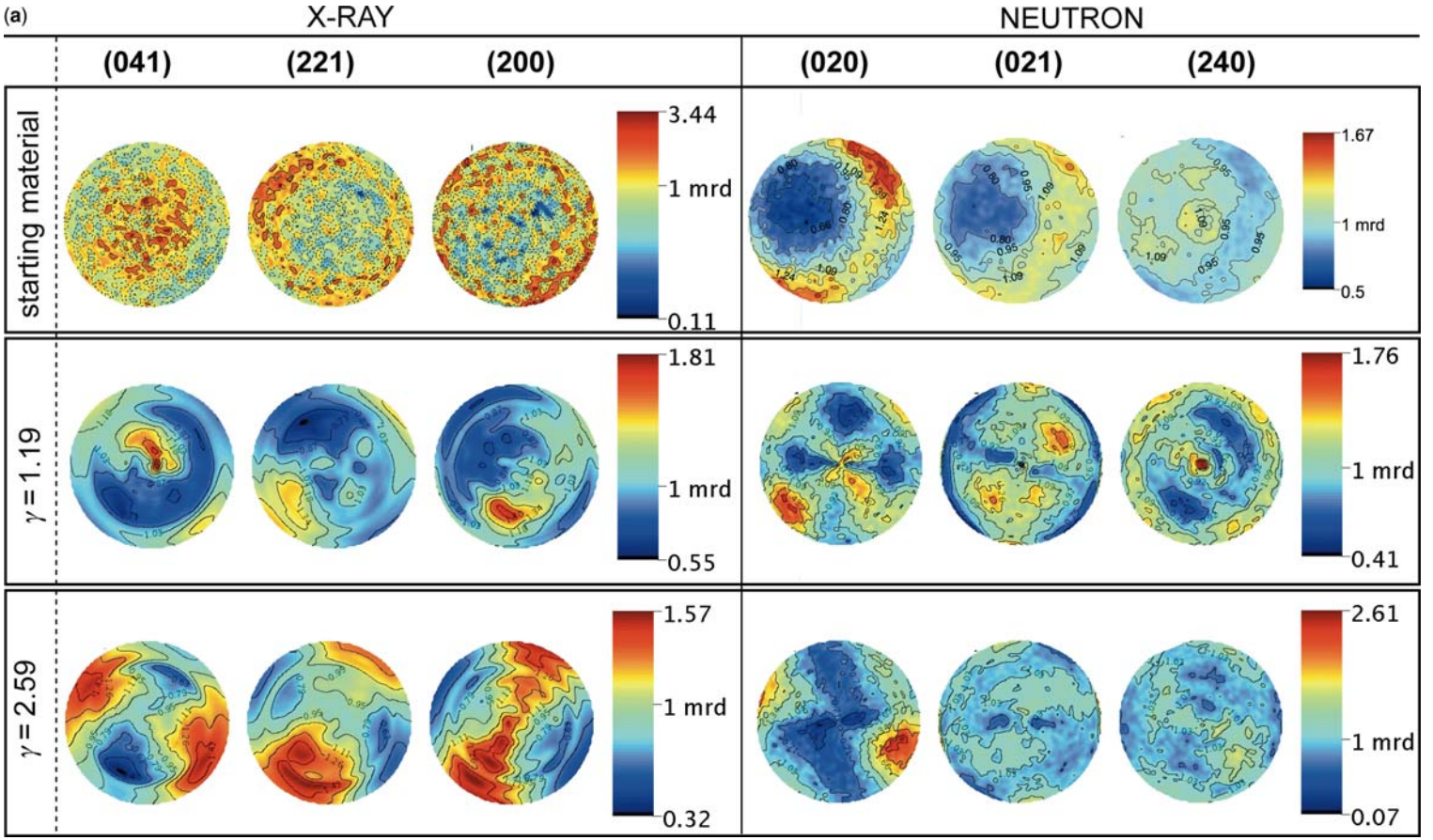

Fig. 6. (**a**) and (**b**) Comparison of the recalculated experimental pole figures for X-ray (041), (221), (200) diffracted planes (left column) and for neutron (020), (021), (240) diffracted planes (right column).

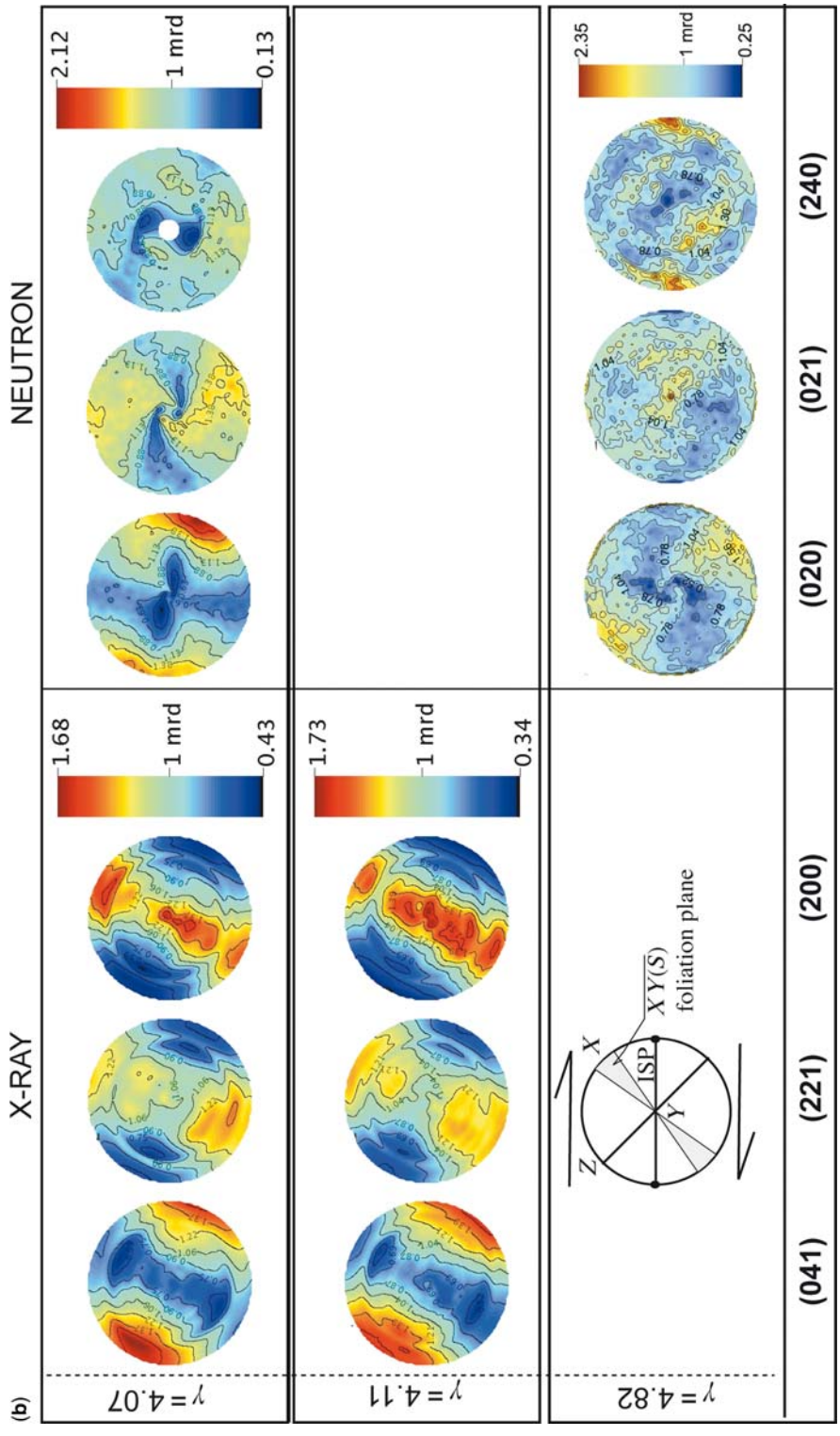

Fig. 6. (*Continued*).

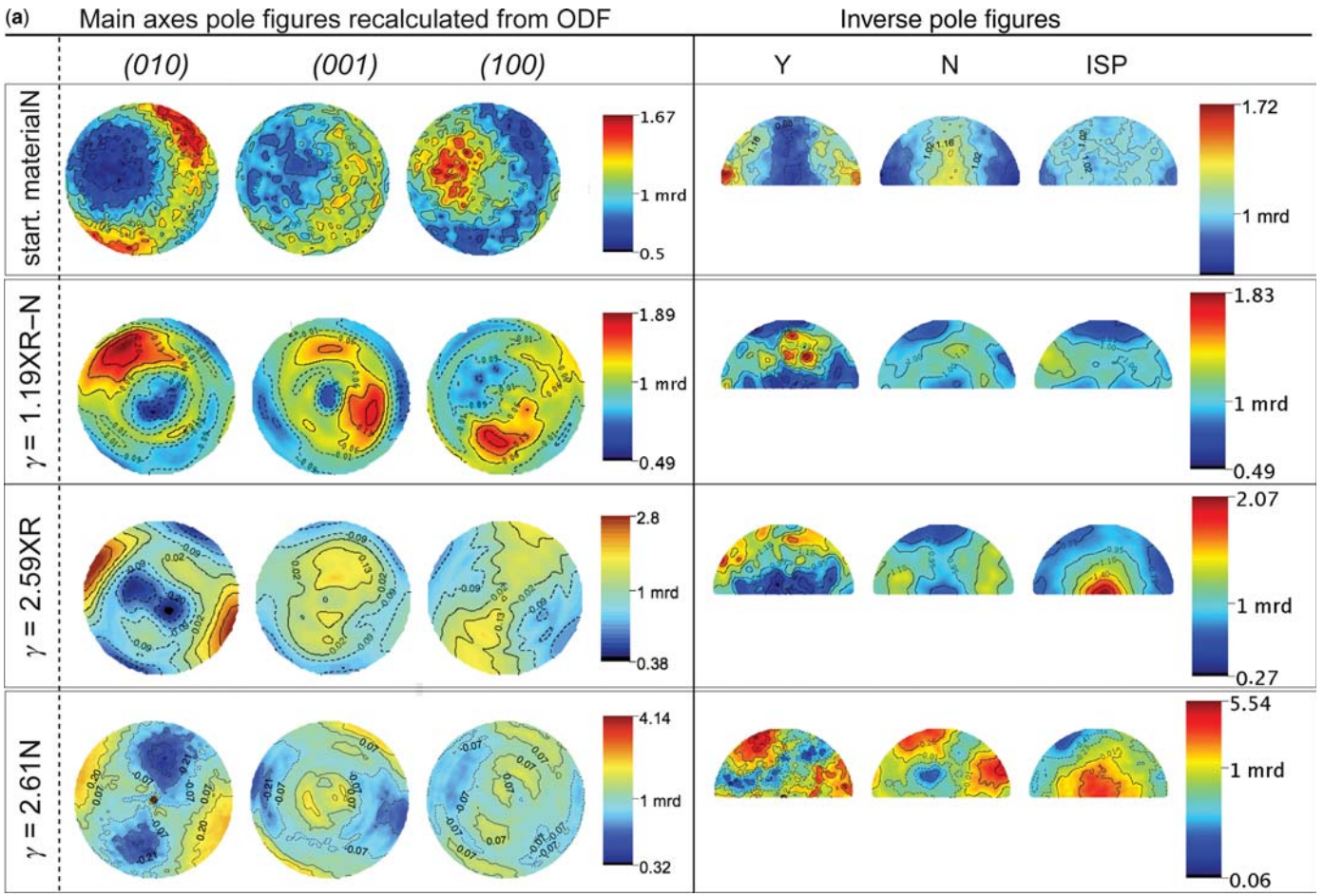

Fig. 7. (**a**) and (**b**) Recalculated pole figures of the main crystallographic planes for X-ray and neutron (left column). Right column shows the inverse pole figures shown in the three main sample directions (Y, N, ISP). Y, Y sample direction; N, normal to ISP direction; and ISP, Imposed shear plane direction.

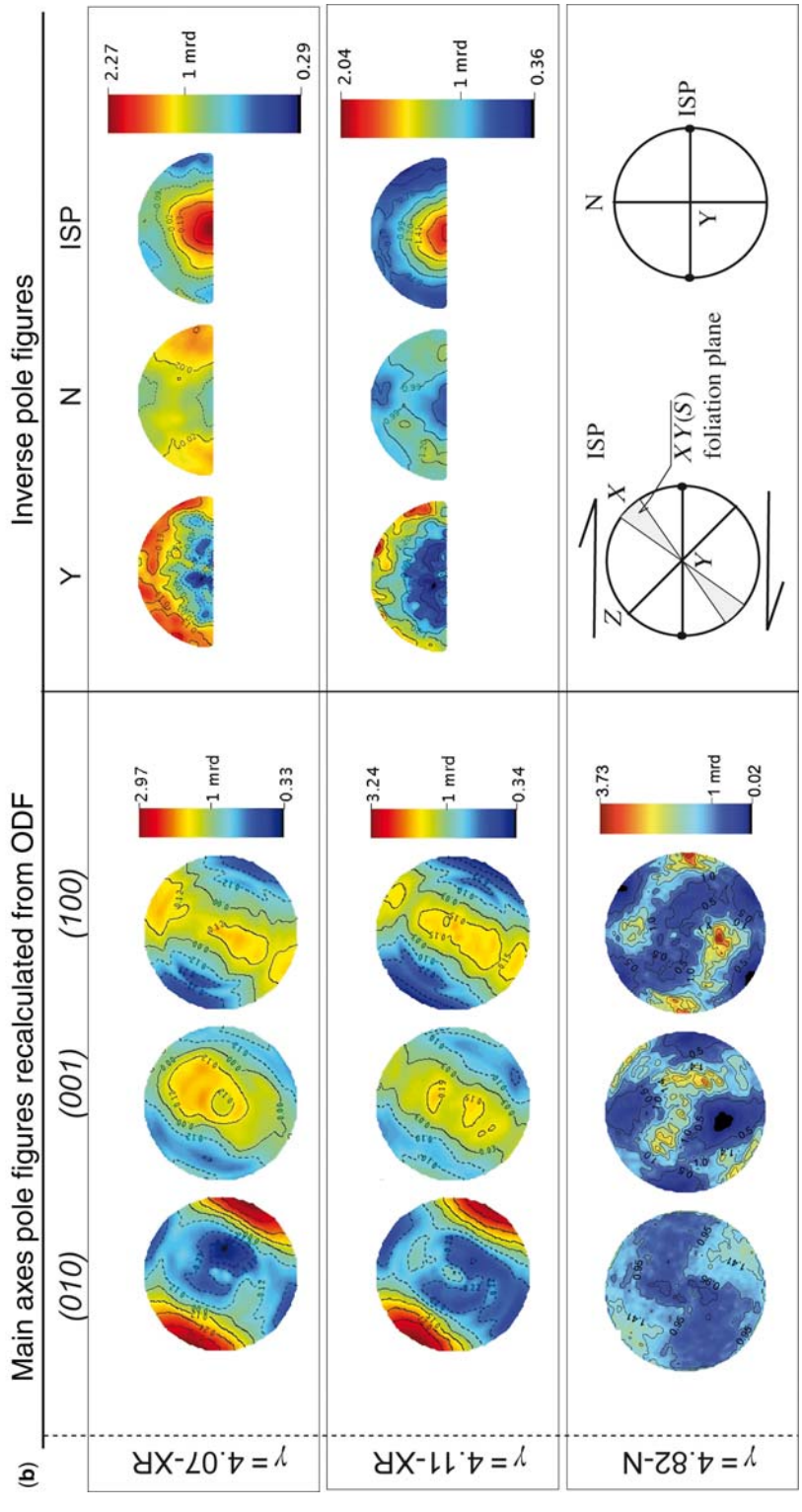

Fig. 7. (*Continued*).

from *Y*. Such preferred orientations increase, attaining higher values of γ. The well-defined (010) and (001) maxima correspond to an incipient girdle distribution of (100) poles at an angle of about 80° with the ISP and mainly parallel to the *X* fabric axis (Fig. 7). Meanwhile the (001) poles show a weak preferred orientation that corresponds to a maximum density within the *XY* plane, close to the *Y* fabric axis. Such a preferred orientation is better developed only at $\gamma > 4.00$, where it becomes closer to a girdle distribution mostly parallel to the *XY*(*S*) plane but still preserving a maximum close to the *Y*-axis. The angular relations given by the pole figures with respect to the ISP and the *XY*(*S*) foliation plane do not change much above $\gamma = 2.50$. These show (010) pole maxima to the ISP angles mainly around 30° in the *XZ* plane, and the corresponding (001) and (100) girdles are perpendicular to the average (010) poles. Consequently, the two latter girdles roughly contain the foliation plane *XY*(*S*). Without deformation, (010) poles are located in the ISP plane parallel to the *Y*-axis, and start deviating from the ISP at $\gamma > 1.00$, reaching its final orientation at 30° from the ISP at larger γ values.

QTA results: neutron diffraction data

A strong maximum of the poles to the (010) planes, which were perfect cleavage planes for gypsum, can be observed at low γ (Fig. 7). This orientation is almost absent within the starting material, whereas it becomes stronger for shear strains of $\gamma > 2.00$. At $\gamma > 1.00$, the (010) poles start moving towards the *Z*-axis at about 30° from the ISP, and correspondingly the (100) and (001) poles distribute progressively on a girdle characterized by maxima that are parallel to the *Y* fabric direction for the (00l) poles or close to the *XY*(*S*) planes for the (*h*00) poles. The (010) pole figure shows two distribution components characterized by two maxima. Such distributions also occur as asymmetrical poles that are stronger for the (001) and (100) pole figures, in which a characteristic small-circle distribution develops from low γ values (e.g. 1.19). At larger γ (e.g. V10 $\gamma = 4.11$) the (010) maximum becomes more defined, together with the corresponding girdle distribution of (001) and (100) poles, even though they still preserve their small-circle distribution. For these neutron pole figures it becomes more complicated to interpret the angles between the pole distribution maxima or girdle axes orientation and the ISP plane or *XY*(*S*) fabric planes. Indeed, as the whole volume of the material is probed by neutrons, the total deformation regimes are seen in the pole figures, with weights that are not determined *a priori*. As the torsion deformation increases, a more and more important volume fraction of deformed rock develops, resulting, for most deformed specimens, in pole figures that resemble the X-ray figures. However, in these figures undeformed or slightly deformed contributions can be observed making the small-circle orientation distribution of the pole figures by integration over the deformation regimes. Inverse pole figures in Figure 7 (right) confirm the relations between ISP and the crystallographic axes observed in direct pole figures. The orientation of the ISP direction is distributed at an angle of about 30° from the [010]-axis (i.e. normal to the pole figure plane) from γ values above 2.00.

Discussion

Evolutionary model

If we consider the experiments and related microstructures, from $\gamma = 0.49$ to $\gamma = 4.82$, as possible steps of a progressive deformational event, we can 'observe' some interesting features during progressive deformation of gypsum within a shear zone at shear strain rates up to $10^{-5}\ s^{-1}$ and $T = 70$–$90\ ^{\circ}C$ at $P = 300$ MPa (Fig. 8).

This microstructural evolution shows that brittle and plastic deformation mechanisms are both active from the beginning of the deformation of gypsum under dextral shear strain (Fig. 8). The progressive evolution of brittle and plastic microstructures, which are well described by geometrical relationships (Figs 2 & 3), describes a coherent evolution from low to high strain. The brittle, Riedel–Tchalenko-like, evolution is characterized by the progressive decrease of α, which describes the relation of *R* planes (Fig. 2a) with the shear plane (i.e. the ISP). At $\gamma > 4.00$ the *R* planes approach the ISP plane and coincide with the *Y* planes of the Riedel-scheme (*R*–*Y* planes in Fig. 2a). Such a negative correlation is broadly shown by α v. γ correlation diagrams (Fig. 4b). The *R*–*Y* planes result more from the progressive evolution of *R* towards the ISP plane than from the development of a second group of planes different from *R*. This is also corroborated by the disappearance of *R* planes at high strains.

However, plastic microstructural features do not change their geometry during the deformation, as shown by the evolution of χ with respect to γ (Fig. 4b). Rather, after an initial decrease, they keep more or less the same orientation or do not show any tendency to reduce the angle between the foliation and the ISP plane, as is generally expected in a monoclinic shear zone (Passchier & Trouw 1996), where the range of χ (from 20° to 45°, Fig. 4) is not related to γ intervals.

At $\gamma > 2.60$ and $T = 90\ ^{\circ}C$ (stages 5 and 6 in Fig. 8) plastic planes occur at low angles with the

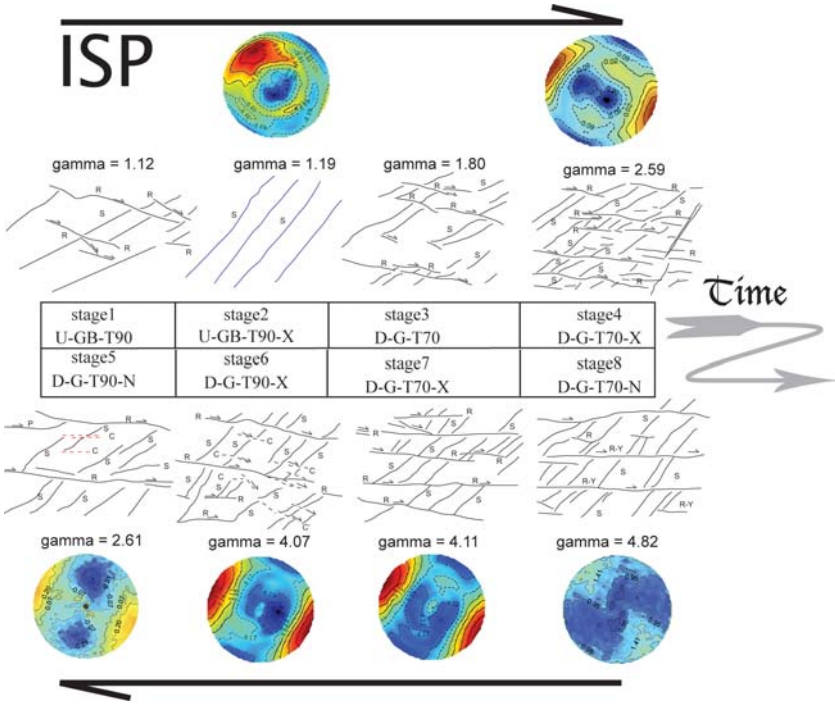

Fig. 8. Schematic representation of the evolution of the modelled shear zone. U, undrained; D, drained; N, neutron; X, X-ray; G, gypsum; B, bassanite; T70, 70 °C; T90, 90 °C. The microstructural evolution shows that brittle and plastic deformation mechanisms are both active from the beginning of the deformation of gypsum under dextral shear strain. However, although plastic microstructural features do not change their geometry during the deformation, brittle features do change their appearance and orientation. Texture analysis shows a well-developed crystallographic preferred orientation of (010) planes starting at the initial deformational stages (e.g. stage 2). This texture becomes stronger during the evolution of the shear zones, but the orientations of the (010) poles does not change substantially above $\gamma = 2$, confirming the similar observations at the microscale.

ISP (i.e. *C* planes), developing the classical *S*–*C* features of mylonitic systems. Similar planes do not develop during stages 4, 7 and 8 at similar or even higher γ values at $T = 70$ °C. These differences can only imply that 70–90 °C is an important temperature interval for the plastic behaviour of gypsum, which most probably starts deforming following the mylonitic scheme (e.g. *S*–*C* system), probably reflecting the activation of new deformation mechanisms and/or slip systems. In contrast, this temperature interval does not seem to be of particular interest for brittle behaviour, as we do not notice any difference in microstructures at this scale of observation. This also implies that across these γ intervals of deforming gypsum, we observe microstructures related to a *brittle plus plastic* deformational system rather than *brittle v. plastic* deformational system or a *brittle–plastic* transition.

Texture analysis (i.e. direct and inverse pole figures) shows a well-developed CPO of (010) planes (Fig. 7) starting at the initial deformational stages (e.g. stage 2 in Fig. 8). This texture becomes stronger during the evolution of the shear zones, but the orientations of the (010) poles does not change substantially above $\gamma = 2$, confirming the similar observations at the microscale. The texture analysis also confirms (Figs 7 & 8) that the preferred slip system is parallel to the (010) planes, although a principal direction of slip (e.g. classical [001] slip direction) cannot be clearly recognized, as shown by the tendency towards girdle distributions of the (100) and (001) poles to planes (Fig. 7).

Conclusions

- We have conducted a quantitative microstructural study on natural gypsum samples that were experimentally deformed in torsion. In this study we compared information derived from optical microstructural analysis and texture analysis obtained by means of diffraction (neutron and X-ray) techniques. With these

techniques we studied samples deformed at temperatures of 70–90 °C and strains (γ) from 0 to 4.82.

- In the microstructural study we could observe, with increasing γ values, the development of an SPO of gypsum aggregates (the *S* foliation) associated with the development and progressive evolution of a Riedel-like brittle deformational scheme. Such brittle microstructures evolve from a relatively early scheme to a substantially completed stage as suggested by the evolution of the angular relationships between the fault planes.
- The brittle evolution is only slightly sensitive to temperature; brittle systems are present in samples deformed at temperatures of 70 and 90 °C, with the difference that in the samples deformed at 90 °C few *C*-like planes occur together with *Y*-like brittle planes. However, the main brittle structure is preserved, suggesting an incipient transition to a plastic deformational regime.
- A plastic deformational regime is also suggested by deformation mechanisms that start to operate at $\gamma > 4.00$ as dynamic recrystallization and grain-size reduction; at greater γ values these deformation mechanisms become more efficient over kinking, passive rotation and mechanical twinning, but still have to compete/collaborate with frictional flow along shear bands. This is also supported by the large difference between the theoretical and actual curves of the finite strain long axis, which implies the counterclockwise rotation due to the sense of shear along the *R* planes.
- From the textural study performed with X-ray and neutron diffraction, we observed that plastic deformation is recorded by gypsum from the initial γ values to highest ones.
- Optical microstructural analysis does not show important differences in the microstructural behaviour of gypsum marking the *S* foliation, while QTA by means of either X-ray and neutron diffraction clearly shows a tendency to reinforce these textures as can be appreciated either from the distribution of maxima and girdles in pole figures or from texture factors.
- There is a general agreement between the X-ray and neutron data, as both show an increasingly strong (010) preferred orientation for increasing γ values. Nevertheless, the results from the X-ray data are much more coherent with the observations from the optical microstructural analysis. The neutron data are controlled by the volume fraction of deformed gypsum. As torsion increases, the deformed volume fraction increases; giving rise, for most deformed specimens, to pole figures that resemble the X-ray figures and that produce the small-circle orientation distribution geometry of the pole figures due to the integration over the deformational regimes.
- Microstructural and textural analyses showed that at the investigated conditions the behaviour of gypsum is completely characterized by a brittle *plus* plastic deformation, while a brittle to plastic transition may be induced, keeping other constraints constant, by increasing the temperature above 90 °C.
- The QTA shows a monoclinic symmetry of the pole figures of gypsum with respect to the ISP (i.e. direct and inverse pole figures). In contrast, the (010) maximum is generally close to the *Z*-axis of the fabric. These symmetries may be used, in the first case, to evaluate the kinematics of the deformation (i.e. sense of shear indicators), while little may be said with respect to the shear sense with respect to the *S* foliation. Where brittle and plastic microstructures coexist, a general sense of shear may be assessed, as shown in this contribution. However, if only plastic microstructures occur, as generally occurs in natural rocks, it is not possible to use texture pole figures (LPO) to assess the sense of shears.

We thank all the technical staff at ILL and CRISMAT. We thank G. Gosso for helpful and extensive discussion. We are truly grateful to E. Rutter and J. Walter, whose reviews helped us to improve the manuscript.

References

ABRAMOFF, M. D., MAGELHAES, P. J. & RAM, S. J. 2004. Image processing with ImageJ. *Biophotonics International*, **11**(7), 36–42.

BARBERINI, V., BURLINI, L., RUTTER, E. & DAPIAGGI, M. 2005. High-strain deformation tests on natural gypsum aggregates in torsion. *In*: BRUHN, D. & BURLINI, L. (eds) *High-strain Zones: Structure and Physical Properties.* Geological Society, London, Special Publications, **245**, 277–290.

BAUMANN, V. W. 1984. Rheologische Untersuchungen an Gips. *Eclogae Geologicae Helvetiae*, **77**, 301–325.

BOEYENS, J. C. A. & ICHHARAM, V. V. H. 2002. Redetermination of the crystal structure of calcium sulphate dihydrate, $CaSO_4 * 2(H_2O)$. *Zeitschrift fuer Kristallographie – New Crystal Structure*, **217**, 9–10.

BUNGE, H. J. & ESLING, C. 1982. Quantitative Texture Analysis. *Deutsche Gesellschaft für Metallkunde*, **551**.

CASTELLANZA, R., GEROLYMATOU, E. & NOVA, R. 2008. An attempt to predict the failure time of abandoned mine pillars. *Rock Mechanics and Rock Engineering*, **41**, 377–401.

CHATEIGNER, D. 2005. Reliability criteria in quantitative texture analysis with experimental and simulated orientation distributions. *Journal of Applied Crystallography*, **38**, 603–611.

CRAKER, W. E. & SCHILLER, K. K. 1962. Plastic deformation of gypsum. *Nature*, **193**, 672–673.

DE MEER, S. 1995. *Deformation Processes in Polycrystalline Aggregates of Gypsum*. PhD thesis, University of Utrecht.

DE MEER, S. & SPIERS, C. J. 1995. Creep of wet gypsum aggregates under hydrostatic loading conditions. *Tectonophysics*, **245**, 171–183.

GRAŽULIS, S., CHATEIGNER, D. *ET AL*. 2009. Crystallography Open Database – an open access collection of crystal structures. A tribute to Michael Berndt. *Journal of Applied Crystallography*, **42**, 726–729.

HARLAND, W. B., MANN, A & TOWNSEND, C. 1988. Deformation of anhydrite–gypsum rocks in central Spitsbergen. *Geological Magazine*, **125**(2), 103–116.

HEARD, H. C. & RUBEY, W. W. 1966. Tectonic implications of gypsum dehydration. *Geological Society of America Bulletin*, **77**, 741–760.

HOXHA, D., GIRAUD, A. & HOMAND, F. 2005. Modelling long-term behaviour of a natural gypsum rock. *Mechanics of Materials*, **37**, 1223–1241.

HOXHA, D., HOMAND, F. & AUVRAY, C. 2006. Deformation of natural gypsum rock; mechanisms and questions. *Engineering Geology*, **86**, 1–17.

KARATO, S. 2008. *Deformation of Earth Materials: An Introduction to the Rheology of Solid Earth*. Cambridge University Press, Cambridge.

KERN, H. & RICHTER, A. 1985. Microstructures and textures in evaporites. *In*: WENK, H. R. (ed.) *Preferred Orientation in Deformed Metals and Rocks; An Introduction to Modern Texture Analysis*. Academic Press, New York.

KO, S. C., OLGAARD, D. L. & BRIEGEL, U. 1995. The transition from weakening to strengthening in dehydrating gypsum: evolution of excess pore pressure. *Geophysical Research Letters*, **22**(9), 1009–1012.

KOCKS, F., TOME, C. & WENK, R. 1998. *Texture and Anisotropy*. Cambridge University Press, Cambridge.

LEISS, B., ULLEMEYER, K. *ET AL*. 2000. Recent developments and goals in texture research of geological materials. *Journal of Structural Geology*, **22** 1531–1540.

LEVYKIN, A. I. & PARFENOV, V. D. 1983. Eksperimenty po derformatsii polikristallicheskogo gipsa. [Experiments of deformation of polycrystalline gypsum.] *Doklady Akademii Nauk SSSR*, **268**, 1190–1192.

LUTTEROTTI, L., CHATEIGNER, D., FERRARI, S. & RICOTE, J. 2004. Texture, residual stress and structural analysis of thin films using a combined X-ray analysis, *Thin Solid Films*, **450**, 34–41.

LUTTEROTTI, L., MATTHIES, S. & WENK, H.-R. 1999. MAUD (Material Analysis Using Diffraction): a user friendly Java program for Rietveld Texture Analysis and more. *Proceedings of the Twelfth International Conference on Textures of Materials (ICOTOM-12)*, **2**, 1599.

LUTTEROTTI, L., MATTHIES, S., WENK, H.-R., SCHULTZ, A. J. & RICHARDSON, J. J. W. 1997. Combined texture and structure analysis of deformed limestone from time-of-flight neutron diffraction spectra. *Journal of Applied Physics*, **81**, 594–600.

MATTHIES, S., LUTTEROTTI, L. & WENK, H.-R. 1997. Advances in texture analysis from diffraction spectra. *Journal of Applied Crystallography*, **30**, 31–42.

MORALES, M., CHATEIGNER, D., LUTTEROTTI, L. & RICOTE, J. 2002. X-ray combined QTA using a CPS applied to a ferroelectric ultrastructure. *Materials Science Forum*, **408–412**, 113–118.

MUEGGE, O. 1898. Uber translationen und verwandte Erscheinungen in Krystallen. *Neues Jahrbuch für Mineralogie*, **1**, 71–154.

OLGAARD, D. L., KO, S. & WONG, T. 1995. Deformation and pore pressure in dehydrating gypsum under transiently drained conditions. *Tectonophysics*, **245**, 237–248.

PANOZZO HEILBRONNER, R. 1993. Controlling the spatial distribution of deformation in experimentally deformed and dehydrated gypsum. *In*: BOLAND, J. N. & FITZGERALD, J. D. (eds) *Defects and Processes in the Solid State: Geosciences Applications*. Elsevier, Amsterdam.

PANOZZO HEILBRONNER, R. & OLGAARD, D. L. 1987. Experimental shear deformation of synthetic gypsum rock. *Terra Cognita*, **7**(1), 64–65.

PANOZZO HEILBRONNER, R. & DELL'ANGELO, L. N. 1990. Fabric development in experimental gypsum shear zones. *Eos, Transactions of the American Geophysical Union*, **71**, 1595.

PASSCHIER, C. W. & TROUW, R. A. J. 1996. *Microtectonics*. Springer, Berlin.

PATERSON, M. S. & OLGAARD, D. L. 2000. Rock deformation tests to large shear strains in torsion. *Journal of Structural Geology*, **22**, 1341–1358.

PEDERSEN, B. F. & SEMMINGSEN, D. 1982. Neutron diffraction refinement of the structure of gypsum, $CaSO_4.2H_2O$. *Acta Crystallographica*, **B38**, 1074–1077.

RANDLE, V. & ENGLER, O. 2000. *Introduction to Texture Analysis: Macrotexture, Microtexture and Orientation Mapping*. CRC Press, Baton Rouge, LA.

RASBAND, W. S. 1997–2008. ImageJ. US National Institutes of Health, Bethesda, MD, USA, World wide web address: *http://rsb.info.nih.gov/ij/*

SCHOFIELD, P. F. & KNIGHT, K. S. 1996. Thermal expansion of gypsum investigated by neutron powder diffraction. *American Mineralogist*, **81**, 847–851.

SNOKE, A. W., TULLIS, J. & TODD, V. R. 1998. *Fault-related Rocks. A Photographic Atlas*. Princeton University Press, Princeton, NJ.

STRETTON, I. C. 1996. *An Experimental Investigation of the Deformation Properties of Gypsum*. PhD thesis, University of Manchester.

TCHALENKO, J. S. 1970. Similarities between shear zones of different magnitudes. *Geological Society of America Bulletin*, **81**, 1625–1639.

TURNER, F. J. & WEISS, L. E. 1963. *Structural Analysis of Metamorphic Tectonites*. McGraw-Hill, New York.

WENK, H.-R. 1985. *Preferred Orientation in Deformed Metals and Rocks; an Introduction to Modern Texture Analysis*. Academic Press, New York.

WENK, H.-R. 2006. Neutron diffraction texture analysis. *Reviews in Mineralogy and Geochemistry*, **63**, 399–426.

YOUNG, R. A. & WILES, D. B. 1982. Profile shape functions in Rietveld refinements. *Journal of Applied Crystallography*, **15**, 430–438.

ZUCALI, M. & CHATEIGNER, D. 2006. Quantitative texture analysis of metadiorites deformed during Alpine subduction; Languard-Campo Nappe-Austroalpines,

Central Alps. *Rendiconti della Societa Geologica Italiana*, **2**, 199–200.

ZUCALI, M., CHATEIGNER, D., DUGNANI, M., LUTTEROTTI, L. & OULADDIAF, B. 2002. Quantitative texture analysis of naturally deformed hornblendite under eclogite facies conditions (Sesia–Lanzo Zone, Western Alps): comparison between X-ray and neutron diffraction analysis. *In*: DE MEER, S., DRURY, M. R., DE BRESSER, J. H. P. & PENNOCK, G. M. (eds) *Deformation Mechanisms, Rheology and Tectonics: Current Status and Future perspectives*. Geological Society, London, Special Publications, **200**, 239–253.

ZUCALI, M., DUGNANI, M., CHATEIGNER, D. & OULADDIAF, B. 2001. Quantitative textural analysis of geological low-symmetry materials: amphiboles from the Sesia–Lanso zone (Italy). *ILL Highlights*, 54–55.